

Proton Electro-Magnetic Form-Factors in the Instanton Liquid Model

P. Faccioli, E. V. Shuryak

Department of Physics and Astronomy, State University of New York, Stony Brook, NY 11794

(November 25, 2018)

We report the first non-perturbative calculation of proton electro-magnetic form-factors in the Random Instanton Liquid Model (RILM) and in the Interacting Instanton Liquid Model (IILM). By calculating the ratio of appropriate three-point to two-point functions, we divide out the coupling constants and compare our results directly to some integral of the form-factors. Using various parametrizations of the electric form-factor $G_E(Q^2)$ at large $Q^2 > 3.5 \text{ GeV}^2$, where it is not yet measured, we compare those with expected theoretical dependence. We find from this comparison that some distributions of charge are clearly excluded (e.g. the same as of the magnetic moment, $\mu G_E/G_M = 1$, as well as the opposite scenario in which $\mu G_E/G_M$ rapidly approach zero), restricting possible behavior of the form-factor to rather narrow band. Furthermore, we found that our calculation of the nucleon form-factors is dominated by a configuration in which two out of three quarks interact with a *single*-instanton, in spite of the fact that the evaluated three-point function has rather large distances ($\sim 1.2 \text{ fm}$) between points. We also estimate the size of the scalar di-quark and found it to be very small, comparable to the typical instanton size.

PAC number(s): 11.15tk

I. INTRODUCTION

The non-perturbative sector of QCD is not yet theoretically understood, and any direct comparison between high accuracy experimental data and theoretical predictions is very valuable. The electro-magnetic form-factors of hadrons are fundamental observables, depending on one scale Q^2 , which are related to the probability of an hadron to absorb a photon and yet remain the same hadron. Apart of telling us much about hadronic sizes and structure, and about the dynamics responsible for the recombination of partons in the final state, form-factors are also supposed to teach us where the transition from the non-perturbative to perturbative regime takes place.

Renewed interest to these issues is triggered by the new precision measurements pursued at the Jefferson Laboratory. Specifically, their new measurements (using a polarization-transfer method) have yielded more accurate proton form-factors, showing for the first time that distributions of charge and magnetic moment are not identical, $\mu G_E/G_M \neq 1$, [1]. The ratio $\mu G_E(Q^2)/G_M(Q^2)$ was measured up to $Q^2 = 3.47 \text{ GeV}^2$ and new data up to $Q^2 \simeq 5.6 \text{ GeV}^2$ should be available soon. These result are plotted at fig. 1 below.

Theoretical arguments about this issues are rather controversial. Apparent agreement between existing data and pQCD power counting [2], [3] ($F_\pi(Q^2) \sim 1/Q^2, G_N \sim 1/Q^4$) have lead some to think that perturbative regime is reached (for a review of pQCD analysis of hadronic form-factors see, e.g. [4]). However, at least in the case of the pion form-factor we do know that the observed value of $Q^2 F_\pi(Q^2)$ is different from its asymptotics at infinite Q^2 , roughly by factor two, and thus some adjustment of its value at higher Q^2 than measured so far should take place.

There are also numerous arguments which show that the origin of the form-factors at $Q^2 < 2 \text{ GeV}^2$ is non-

perturbative. Historically, the first calculations of this kind for the proton form-factors were based on the Operator Product Expansion and QCD sum-rule analysis, supplemented by the assumption of vacuum dominance [5,6,8]. In this approach all information about the non-perturbative properties of the QCD vacuum are parametrized via few quark and gluon condensates. However, this approach is only valid at small enough distances, and in order to extract physical observables one is then forced to consider complete experimental spectral densities which includes contributions from multiple excited states, not just pion or nucleon alone. To overcome this difficulty, a simple ‘‘pole-plus-continuum’’ (PPC) model for the spectral representation is often adopted. Unfortunately, that introduces significant model dependence in the analysis and reduces its predictive power. In practice, this approach is not always successful: for example the sum-rule calculation of the proton’s two-point function involving a PPC ansatz agrees with the experimental data, only if a particular Ioffe current is used [7].

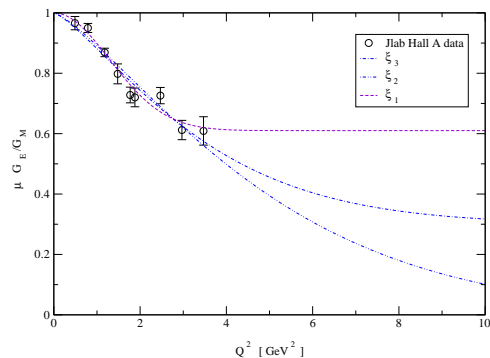


FIG. 1. JLAB results for $\mu G_E/G_M$ [1] as compared to the fits (20) with (21).

In general, hadronic data usually tell us about long-distance behavior, while field theoretic calculations have better predictive power in the opposite limit of small distances. One issue any application of such method has to face is the *existence* and size of the “*working window*” of distances in which a quantitative comparison between the two can be made. To be successful, a theoretical approach has to be able to predict the correlation functions at relatively large ($\sim 1fm$) distances: then the unknown contribution from all excited states is automatically suppressed and only the pole corresponding to the lowest lying particle survives. Two illustrative examples of relative strength of both components, for two-point isovector pseudoscalar current correlator (“pion”) and the nucleon (with current to be specified below) are shown in Fig.2 as a function of (Euclidean) distance l between the currents. Here and below, all correlators are normalized to their free quark value (so unit value at small l means just free quark motion, a simple consequence of asymptotic freedom). From those examples one can see, that the pole dominance is rapidly reached at some (channel-dependent) value of l , about $0.8 fm$ for the nucleon.

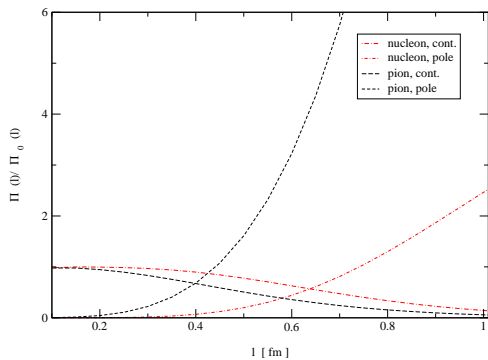


FIG. 2. Pole and continuum contributions for the pion [18] (dashed, $s_0 = 1.6 GeV^2$) and nucleon (dot-dashed, $s_0 = 2.5 GeV^2$) two-point correlation functions.

The most direct way of calculating *ab initio* such correlation functions is numerical lattice-based approach. However, quite successful results were also obtained from much simpler instanton-based models, see review [9] and also [10] for recent example of quantitative predictions of the model, compared to the τ lepton decay data. Closest to the present work is the successful calculation of the pion form-factor [17,16] using the same instanton-based model as used below. One important aspect of [16] is the direct relation found there between the pion and instanton sizes.

In the present work we try to answer the following questions. How to organize the calculation, what are the best combination of three and two-point correlators to be used? At what distances those should be calculated, in order to exclude contributions of the nucleon excited states? How do the results obtained correlate with exper-

imental form-factors? Are they sensitive to the high- Q^2 part which is not yet measured, and if so, can we make some predictions? Can the proton form-factors be described in terms of configurations of three valence quarks bound by instanton forces? Are these dominated by one single instanton, at least at some scale? If so, do all three quarks interact strongly with it, or only two, as arguments based on Pauli principle for zero modes would suggest? And finally, how does this approach correlate with phenomenological models of the nucleon, such as quark-diquark model?

The paper is organized as follows. In section II, we will present our results for the nucleon two-point and electro-magnetic three-point function, obtained in the Random Instanton Liquid Model (RILM), in the Interacting Instanton Liquid Model (IILM) and in the Single Instanton Approximation (SIA). In section III we show how such correlation functions can be evaluated from the phenomenological knowledge of proton mass and form-factors and we compare them with our theoretical predictions. In section IV we discuss the physical implications of our calculations, in particular in relation to different hadronic models of the nucleon. Results and conclusions are summarized in section V.

II. CALCULATION OF THE CORRELATION FUNCTIONS FROM THE INSTANTON LIQUID MODELS.

Our theoretical investigation is based on the analysis of two and three-point Euclidean correlation functions, in coordinate space. In particular we consider the electromagnetic three-point function:

$$\Pi_{sc4}(x, y) = \langle 0 | \text{tr} [\eta_{sc}(x/2) J_4^{em}(y) \bar{\eta}_{sc}(-x/2) \gamma_4] | 0 \rangle, \quad (1)$$

where $J_4^{em}(y)$ is the fourth component of the electromagnetic current,

$$J_\mu^{em}(y) := \frac{2}{3} \bar{u}(y) \gamma_\mu u(y) - \frac{1}{3} \bar{d}(y) \gamma_\mu d(y). \quad (2)$$

$\eta_{sc}(x)$ denotes a particular combination of Ioffe currents, that we refer to as the scalar current:

$$\eta_{sc}(x) := \epsilon_{abc} [u^a(x) C \gamma_5 d^b(x)] u^c(x), \quad (3)$$

where a, b, c are color indices. In principle, one can choose any linear combination of Ioffe currents, which excite states with the same additive quantum numbers of the proton (as well as states with opposite parity). Our choice is theoretically motivated by the fact that $\eta_{sc}^c(x)$ contains explicitly a di-quark term, which was shown to receive maximal coupling to instanton’s zero modes [9].

The nucleon coupling to such current is defined as

$$\langle 0 | \eta_{sc}(x) | p, s \rangle = \Lambda_{sc} u(p, s) e^{-iqx}, \quad (4)$$

where $u(p, s)$ is a Dirac spinor and s is the spin index.

Let us specialize now a particular choice¹ for the three-point function (1), in which:

$$\begin{aligned} y \cdot x &= 0, & \text{and} \\ l &:= |y| = |x|. \end{aligned} \quad (5)$$

We shall consider also the following two-point Euclidean proton correlation function

$$\Pi_{sc}(x) = \langle 0 | \text{Tr} [\eta_{sc}(x/2) \bar{\eta}_{sc}(-x/2) \gamma_4] | 0 \rangle, \quad (6)$$

in which the propagation can be chosen along the Euclidean time axis. Due to the presence of γ_4 , this correlator receives contribution from two quark zero-modes propagators in the field of an instanton². Notice that, in a theory with two massless flavors, this is the maximal number allowed by Pauli principle.

Since the same factor Λ_{sc}^2 , which can not be determined from experiments, appears both in the expression for the proton two-point function (6), and in three-point function (1), it is natural to consider the ratio:

$$\Gamma(l) := \frac{\Pi_{sc4}(l, l)}{\Pi_{sc}(l)}, \quad (7)$$

in which such factor is divided out. In the next section we show that $\Gamma(l)$ for $l \gtrsim 0.7 fm$ depends only on the the proton's mass and form-factors. At this scale, $\Gamma(l)$ is dominated by non-perturbative effects and therefore represents a suitable tool to probe model descriptions of the non-perturbative strong dynamics.

In instanton models, one assumes that the Euclidean QCD partition function is saturated by the configurations of an interacting ensemble of pseudo-particles (instantons and anti-instantons) which, in ordinary Minkowski space, are associated to the tunneling between degenerate classical vacua.

Each configuration of the ensemble is determined by a set of collective coordinates, specifying the the position, the size and the orientation in color space of each instanton.

The parameters of the model are the average instanton size, $\bar{\rho} \simeq 1/3 fm$ and the average instanton density, $\bar{n} \simeq 1 fm^{-4}$. These values have been determined from several phenomenological studies [20], [9] as well as from lattice simulations [21].

In the Random Instanton Liquid Model (RILM), one assumes that all instantons have the same size and that the distribution of all remaining collective coordinates is

completely random. In the Interacting Instanton Liquid Model (IILM) the distribution is calculated from numerical simulation of the partition function, describing interaction between instantons. The most important and complicated part of this interaction is fermion exchanges between them, described by the fermionic determinant in the partition function.

Both the RILM and IILM have been shown to have nucleon as a bound state, and give reasonable values for the its mass [9]. Furthermore, these models provide very different nucleon (octet) and delta (decuplet) correlators, explaining the splitting between the nucleon and the delta in terms of zero mode forces [12], [13]. Another important result of these works is the prediction of the nucleon coupling constants to Ioffe current: it is proportional to the probability to find all three quarks at the same point, and is needed for such applications as evaluation of proton decays.

As the first step toward understanding of the function $\Gamma(l)$ we have evaluated it analytically in the Single Instanton Approximation (SIA), in which only the closest instanton is taken into account explicitly [20], [23]. In such an approach, the correlation functions are evaluated from the the quark propagator $S_{I(A)}(x, y)$ in the instanton (anti-instanton) background. This is known exactly to be the sum of two terms: a zero-mode part, $S_{zm}(x, y)$ and a non-zero mode part, $S_{nzm}(x, y)$. In most applications, $S_{nzm}(x, y)$ can be approximated with the free propagator, $S_0(x, y)$, while the quark zero-mode propagator reads:

$$S_{zm}(x, y) = \frac{\psi_0(x) \psi_0^\dagger(y)}{-i m}, \quad (8)$$

where $\psi_0(x)$ represents an eigenmode of the Dirac operator³ with vanishing eigenvalue (quark zero-mode),

$$i \not{D} \psi_0(x) = 0, \quad (9)$$

$$\begin{aligned} \psi_{0 \alpha \nu}(x; z) &= \frac{\rho}{\pi} \frac{1}{((x-z)^2 + \rho^2)^{3/2}} \cdot \\ &\cdot \left[\frac{1 - \gamma_5}{2} \frac{\not{x} - \not{z}}{\sqrt{(x-z)^2}} \right]_{\alpha \beta} \cdot U_{ab} \epsilon_{\beta b}, \end{aligned} \quad (10)$$

(here z denotes the instanton position, $\alpha, \beta = 1, \dots, 4$ are spinor indices and U_{ab} represents a general group element).

In [23] we showed that, if the correlation function receives contribution from at least two quark zero-mode propagators, one can incorporate the effects of all other

¹Notice that, in such configuration, the vertices $x/2$, $-x/2$ and y do not lie on the same line. The convenience of such choice will be discussed in the next section.

²This can be verified by simply counting the quark chirality flips.

³The explicit expression for $\psi_0(x)$ is, of course, gauge dependent. The ILM is formulated in the singular gauge, where the topological charge is localized around each instanton.

instantons in an effective mass term that replacing the current mass in (8). More specifically, correlation functions receiving contribution from two zero-mode propagators will be proportional to inverse powers of the current quark mass, m^2 , which will be replaced by an effective parameter m_2^2 . Such parameter depends on the ensemble and has been determined to be $m_2^2 \simeq (65 \text{ MeV})^2$ for the RILM and $m_2^2 \simeq (105 \text{ MeV})^2$ for the IILM. The resulting expressions for $\Pi_{sc}(l)$ and $\Pi_{4sc}(l, l)$ are ⁴:

$$\Pi_{sc}(l) = \frac{15}{\pi^6 l^9} + \frac{12 \bar{n} \rho^4}{l^3 \pi^4 m_2^2} \int d^4 z \cdot \frac{1}{[\bar{z}^2 + (z_4 - l)^2 + \rho^2]^3 [\bar{z}^2 + z_4^2 + \rho^2]^3}, \quad (11)$$

and

$$\Pi_{4sc}(l, l) = \frac{96}{25 \pi^8 l^{12}} + \frac{4 \bar{n} \rho^4}{l^6 15 \pi^8 m_2^2} \int d^4 z \cdot \frac{1}{[(l/2 + z_4)^2 + \bar{z}^2 + \rho^2]^{3/2} [(l/2 - z_4)^2 + \bar{z}^2 + \rho^2]^{3/2}} \cdot \left\{ \frac{8}{[(l/2 + z_4)^2 + \bar{z}^2 + \rho^2]^{3/2} [(l/2 - z_4)^2 + \bar{z}^2 + \rho^2]^{3/2}} + \frac{7/5}{[(l - z_2)^2 + Z^2 + \rho^2]^{3/2} [(l - z_2)^2 + Z^2]^{1/2}} \cdot \left(\frac{2l^2 + 5lz_4 + \bar{z}^2 + 2z_4^2 - 4lz_2}{[(l/2 - z_4)^2 + \bar{z}^2 + \rho^2]^{3/2} [(l/2 + z_4)^2 + \bar{z}^2]^{1/2}} + \frac{2l^2 - 5lz_4 + \bar{z}^2 + 2z_4^2 - 4lz_2}{[(l/2 + z_4)^2 + \bar{z}^2 + \rho^2]^{3/2} [(l/2 - z_4)^2 + \bar{z}^2]^{1/2}} \right) \right\}, \quad (12)$$

where $\bar{z}^2 := z_1^2 + z_2^2 + z_3^2$ and $Z^2 := z_2^2 + z_3^2 + z_4^2$.

Note, that contribution from all other instantons enters only via an effective mass parameter. Although the values of these effective masses in RILM and IILM are quite different. Fortunately, one finds that two and three-point functions have the same power of this parameter, and thus it actually drops out in our ratio $\Gamma(l)$ as soon as the perturbative (free) contribution becomes negligible.

The SIA is supposed to break down when quarks are propagating for distances larger than the typical separation between two neighbor instantons ($\sim 1 \text{ fm}$). Nevertheless, in [23] we showed that the SIA calculations for hadronic two-point functions agree with the

⁴Our theoretical calculations for $\Pi_{4sc}(l, l)$ have been obtained retaining only connected diagrams. This is motivated by the fact that all one-instanton contributions to the disconnected diagrams for the electro-magnetic three-point function are mqzero.

corresponding ILM results up to quite large distances ($\sim 0.7 \div \sim 1 \text{ fm}$, depending on the correlation function) so there may be a window for such an approach in the present calculation. In figs. 9 and 10 we have plotted the ratios $\Pi_{sc}(l)/\Pi_{sc \text{ free}}(l)$ and $\Pi_{4sc}(l, l)/\Pi_{4sc \text{ free}}(l, l)$ obtained in the SIA and from numerical simulations in the RILM and IILM ⁵. It is quite surprising to notice that the SIA results for three-point functions reproduce the corresponding ILM result all the way up to 1.2 fm . For larger distances statistical errors on ILM results make the comparison somewhat meaningless.

Now we make the second step, and numerically evaluate the function $\Gamma(l)$ from a random and an interacting instanton ensembles. In both cases we used propagators which include complete re-diagonalization in the zero-mode subspace. We have used 256 instantons and anti-instantons in a $(4 \text{ fm})^4$ periodic box. The results are presented in fig. 3: one can see that, although the IILM and the RILM give different two-point and three-point correlation functions (see figs. 9 and 10), their ratio $\Gamma(l)$ is essentially the same.

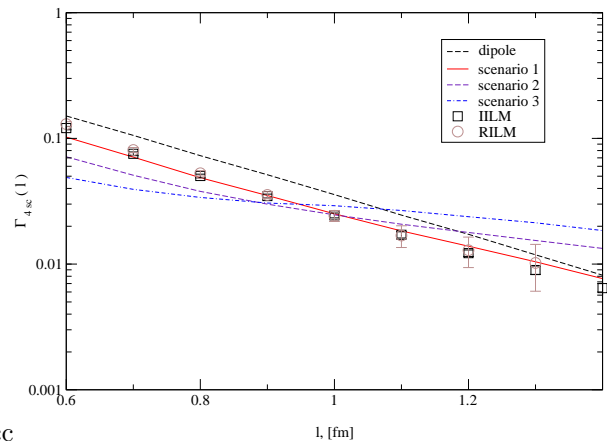


FIG. 3. Large distance behavior of $\Gamma(l)$. The lines represent the contribution of the nucleon pole, for the different scenarios given by (20) and (21). In particular, the solid line corresponds to the scenario 1, where the ratio $\mu G_E/G_M$ stabilizes at around 0.6 at high Q^2 , while the large-dashed line was obtained using the dipole formula for *both* G_M and G_E . The circles (squares) represent RILM (IILM) predictions.

⁵In producing these plots we have used the effective mass parameters defined and evaluated in [23].

III. RELATING THE EUCLIDEAN CORRELATION FUNCTIONS WITH THE EXPERIMENTAL DATA

In a field theoretic Euclidean framework (such as lattice QCD or instanton-based models) a very important step is to encode available information about masses, form-factors, wave functions and other properties of particular hadrons into appropriate Green functions.

The spectral representation of correlators can be traditionally written assuming a ‘‘pole-plus-continuum’’ ansatz for the spectral density:

$$\Pi_{sc}(x) = -(\Lambda_{sc})^2 D'(M_N, x) - \frac{1}{64\pi^4} \int_{s_0}^{\infty} ds s^2 D'(\sqrt{s}, x), \quad (13)$$

Here the first term represent the nucleon contribution: M_N is the nucleon mass and $D(m, x)$ is the Euclidean scalar propagator of a particle of mass m .

The second term represents the contribution of the excited states with nucleon quantum numbers (including those with opposite parity). This particular form of ‘‘continuum contribution’’ represents parton-hadron duality, it corresponds to the discontinuity of the perturbative (free) quark loop diagram contributing to the same correlation function. The new parameter s_0 identifies the threshold for the onset of the duality regime: at this energy transition from the non-perturbative to the perturbative regime takes place. The QCD sum rules practitioners obtain the value for this parameter together with others (masses and coupling constants), from comparing theoretical and experimental dependence of the correlator. However, the results still depend on this specific assumption about the contribution of the excited states.

We have chosen not to deal with this uncertainty, calculating all correlation functions at sufficiently large distances $x \gtrsim 1fm$, where the continuum contribution is negligible compared to nucleon contribution. (see fig. 2).

The contribution to (1) due to the nucleon pole can be evaluated in terms of the Fourier transforms of the Dirac and Pauli form-factors (see appendix A for the detailed derivation):

$$\Pi_{sc4}(x, y) \stackrel{|x|, |y| \gg 1}{\rightarrow} \Lambda_{sc}^2 \int d^4z Tr \left[S_{M_N} \left(\frac{x}{2}, y+z \right) \left[\gamma_4 F_1(z) + \frac{i\sigma_{4\nu}}{2M_N} F_2^\nu(z) \right] S_{M_N} \left(y+z, -\frac{x}{2} \right) \gamma_4 \right], \quad (14)$$

where $S_{M_N}(x, x')$ denotes the nucleon propagator from x' to x and

$$F_2^\nu(z) := i \partial^\nu F_2(z) = \frac{i z^\nu}{|z|} F_2'(z). \quad (15)$$

Eq. (14) has a simple physical interpretation (see fig. 4): at large distances, the three-point function (1) represents the (Euclidean) amplitude for a finite-sized nucleon to be created at $-x/2$, to absorb a photon at y and

be annihilated at $x/2$. Notice that the electro-magnetic vertex depends on the Fourier transforms of the Pauli and Dirac form-factors and therefore contains information about the shape of the proton.

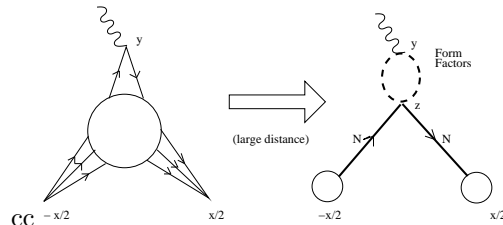


FIG. 4. In the large distance limit, the three-point function Π_{Sc4} is dominated by the nucleon pole.

In order to evaluate $\Pi_{sc4}(x, y)$, we need an expression for $F_1(z)$ and $F_2(z)$. This can be obtained by Fourier transforming the analytic continuation to Euclidean space of the fits of the experimental form-factors. Typically, elastic scattering experiments allow to obtain the Sachs electric and magnetic form-factors, which are related to the Pauli and Dirac form-factors by:

$$G_E(Q^2) = F_1(Q^2) - \tau F_2(Q^2) \quad (16)$$

$$G_M(Q^2) = F_1(Q^2) + F_2(Q^2), \quad (17)$$

where $\tau := Q^2/4M^2$ and $Q^2 = -q^2$.

At low momenta, $Q^2 \lesssim 1 GeV^2$, $G_E(Q^2)$ and $G_M(Q^2)$ can be extracted from usual Rosenbluth separation method and error-bars are of the order of a few percent. In this regime, the data for both form-factors are well fitted by the so-called dipole formula,

$$G_M(Q^2)/\mu \simeq G_E(Q^2) \simeq G_D(Q^2), \quad Q^2 \lesssim 1 GeV^2 \quad (18)$$

where

$$G_D(Q^2) = \frac{1}{(1 + \frac{Q^2}{0.71})^2}, \quad (19)$$

and μ is the proton magnetic moment.

As the momentum increases, the cross section becomes dominated by G_M making the extraction of G_E more and more difficult. As a result, error-bars on G_E become very large already at $Q^2 \sim 2 GeV^2$ while error-bars on G_M remain small up to $Q^2 \simeq 30 GeV^2$ [19].

Using this experimental information we are now able to complete our phenomenological estimate of the relevant three-point function. The coordinate representation of G_M has been obtained by Fourier transforming the dipole fit (18), which is very accurate at the momentum scale we are interested in. The fit for G_E can be obtained as follows. One can assume the following ansatz:

$$G_E(Q^2) = G_D(Q^2) \xi(Q^2), \quad (20)$$

where the function $\xi(Q^2)$, which accounts from the deviation from dipole shape, can be obtained from the available data for $\mu G_E/G_M$. These can be well reproduced by the following set of exponential fits which, however, have different trends in the kinematical region $Q^2 > 3.5 \text{ GeV}^2$ (see fig. 1):

$$\begin{aligned} \xi_d(Q^2) &= 1. & (\text{dipole parametrization}) \\ \xi_1(Q^2) &= 0.39 e^{-\frac{(Q^2)^2}{3.12}} + 0.61. \\ \xi_2(Q^2) &= 0.70 e^{-\frac{(Q^2)^{1.3}}{5.39}} + 0.30 \\ \xi_3(Q^2) &= e^{-\frac{(Q^2)^{1.3}}{8.71}} \end{aligned} \quad (21)$$

The corresponding functions $F_1(z)$ and $F_2(z)$ are plotted in fig. 5 and fig. 6.

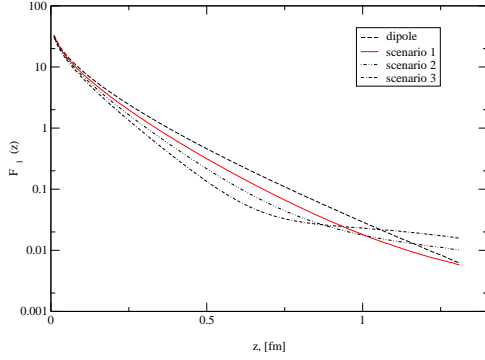


FIG. 5. Fits of the Pauli form-factor (F_1) in coordinate representation obtained using the parametrization (21)

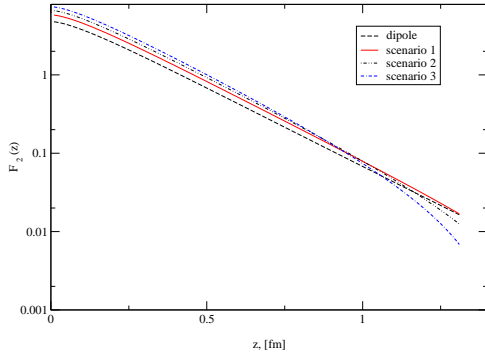


FIG. 6. Fits of the Dirac form-factor (F_2) in coordinate representation obtained using the parametrization (21)

The results of our phenomenological calculation for $\Gamma(l)$, using the parametrization (21) for $\xi(Q^2)$ are reported in fig. 3. It is important to recall that our phenomenological calculation of $\Gamma(l)$ is valid only at large

distances, where the proton pole is dominant. We therefore need to estimate how large l needs to be for this assumption to hold. From the analysis of the two-point function, we have seen that the continuum contribution is almost completely suppressed for $l \gtrsim 1 \text{ fm}$. In the electro-magnetic three-point function, however, one of the quarks is struck in the point y , acquiring an undetermined amount of momentum. As a result, at such vertex the nucleon pole gets mixed with all other resonances and one needs to wait for another $\sim 1 \text{ fm}$, in order for the pole to decouple again. From this rough estimate, one expects that (1) can be identified with (14) if the three quarks have propagated for about 2 fm . In the ILM and on the lattice, the vacuum is usually simulated in a four-dimensional periodic box, whose maximal size is determined by the machine's precision and by computational time constraints. It is therefore important to make a convenient choice of x and y in (1). In particular, we need to consider three-point functions that are large enough for the ground-state pole to decouple but can be fit into a relatively small box. At this purpose, it is generally a good idea to let quarks propagate along the diagonals. With the choice (5) one has that the quarks travel for the needed $\sim 2 \text{ fm}$ already for $l \sim 0.7 \text{ fm}$.

At this point, we may ask to what momentum scale is our analysis in configuration space sensitive to. From uncertainty principle arguments, one would naively expect that correlation functions of size l should be essentially sensitive to the physics at the scale $Q \sim 1/l$. Along this line, one is then led to argue that our large sized ($l > 0.7 \text{ fm}$) correlation functions can only be used to study to the small momentum part of the form-factors. This is certainly true asymptotically: for example, in the (numerically infeasible) limit of extremely large l , the three-point function should depend only on the proton electric charge and magnetic moment and, therefore, all scenarios considered in (21) must give the same answer. However, at intermediate distances the situation is more complicated. In fact, eq. (14) shows that $\Pi_{sc4}(l)$, is related through a non-trivial integral to the Fourier transform of the form-factors (eq. 14). Such integration mixes the different modes in such a way that three-point functions with $l > 0.7 \text{ fm}$ are still quite sensitive to the shape of form-factors at high Q^2 . This is already seen in fig. 7, where $\Pi_{4sc}(l, l)$, obtained from fits of the form-factors that differ only in the high momentum range ($Q^2 > 3.5 \text{ GeV}^2$) are compared. Clearly, such green functions at, say, $l \sim 1.5 \text{ fm}$ are quite different and larger distances are needed for the three curves to converge.

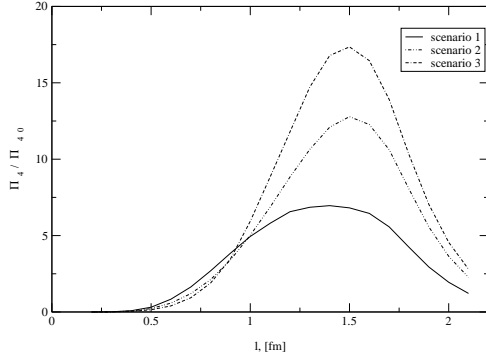


FIG. 7. Proton pole contribution to the Electro-magnetic three-point function $\Pi_{4,sc}$, obtained from three different fits for $\mu G_E/G_M$ (eq. 21) which differ only for $Q > 3.5 GeV^2$.

It is interesting to further analyze the contribution of different momentum components to our correlator. At this purpose, in fig. 8 we have plotted the three-point function corresponding to scenario 1, and we compare it with two more curves, that one obtains from the same parametrization, but keeping only the contribution from $Q < 1 GeV$ and $Q > 1 GeV$ to the form-factors $F_1(z)$ and $F_2(z)$ (see eq. A7). From this figure we clearly see that some non trivial cancellations occur and the high momentum components of the form factors play an important role in the whole range of l considered.

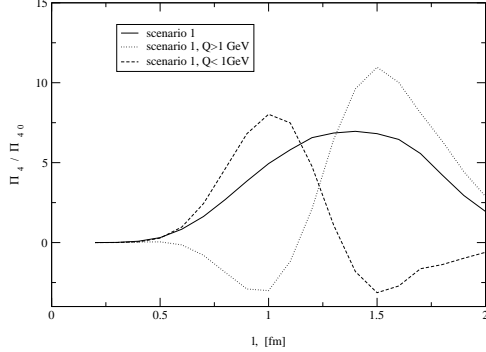


FIG. 8. Contribution of different momenta to the proton electro-magnetic three-point function $\Pi_{4,sc}$. The solid line represents the correlators obtained in scenario 1, integrating over all momenta, the dotted (dashed) line is obtained keeping only the $Q > 1 GeV$ ($Q < 1 GeV^2$) components of the form-factors.

Now we are ready to compare theoretical calculations for (7) to the four curves corresponding to different “scenarios” for the electric form-factor behavior at large Q^2 . First of all, one finds that the overall magnitude and qualitative behavior with l are similar. This is very non-trivial, since there are compensations between electric versus magnetic, and small versus large Q^2 .

Furthermore, our results seem to be able to distinguish

between various “scenarios”. In fact, the scenario 0 (in which $G_E \mu/G_M = 1$, identically) and the scenario 3 (in which $G_E \mu/G_M$ rapidly approaches zero) seem to be ruled-out, assuming the theory prediction is correct. Best agreement seem to be reached for the scenario 1, the case in which $G_E \mu/G_M$ falls with Q^2 till about 0.6, as found by Jlab experiment, and then more or less stabilizes at large momenta. Scenarios in which the ratio stabilizes at similar values are of course also possible.

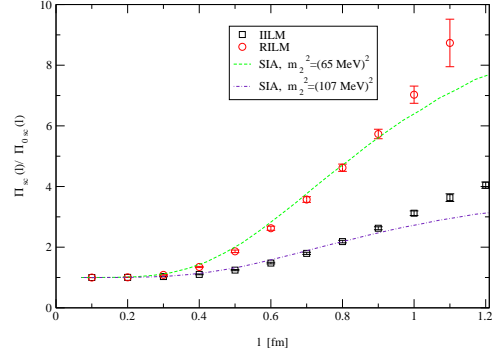


FIG. 9. Proton two-point function, $\Pi_{sc}(l)$ evaluated in the ILM and in the SIA. The circles (squares) correspond to RILM (IILM) results. Dashed (dot-dashed) lines correspond to SIA results using the mass parameters evaluated in [23]: $m_2^2 = (65 MeV)^2$ ($m_2^2 = (107 MeV)^2$).

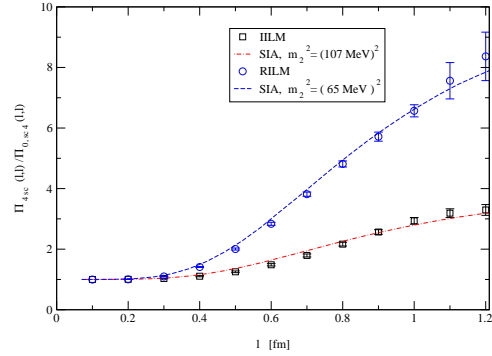


FIG. 10. Proton three-point function, $\Pi_{4,sc}(l)$ evaluated in the ILM and in the SIA. The circles (squares) correspond to RILM (IILM) results. Dashed (dot-dashed) lines correspond to SIA results using the mass parameters evaluated in [23]: $m_2^2 = (65 MeV)^2$ ($m_2^2 = (107 MeV)^2$).

IV. DISCUSSION AND COMPARISON WITH HADRONIC MODELS

After having calculated of the relevant Green functions, analytically in SIA and numerically for the ensembles, and compared our prediction with the data, let us

go into somewhat more general discussion of the physics involved.

First let us ask, why RILM and IILM give so close results for the ratio $\Gamma(l)$, but not the correlators themselves? The former model has no correlation between instantons while the latter has strong ones⁶ and their predictions are usually not that close. The reason is that (see also discussion in section II), at the scale we are working at, the correlation functions are dominated by *one single instanton*.

This implies two important consequences. First, there actually exists a “working window” where the (unknown) continuum contribution is highly suppressed and yet SIA is still accurate. Second, since the only relevant dimensional parameter in SIA is the instanton size ρ (the instanton density also drops out in the ratio), it follows that the scale of the nucleon form-factor is completely determined by it⁷.

The content of the typical nucleon configuration is pictured phenomenologically in different ways: e.g. the usual quark model picture is that of three massive “constituent” quarks, bound by confining forces. Another possibility discussed in literature is as a loose bound state of a quark with a scalar system of two quarks, more tightly bound (di-quark). In this section, we consider the problem of qualitatively determining the size of such di-quark, in the instanton-based models.

From the Pauli principle on the level of instanton zero modes, only two (u and d) of the three quarks can be in the state described by the zero-mode wave-function (10) and therefore be localized around the closest instanton. As a result, the typical size of the di-quark should be determined by the size of the instanton, and be generally comparable to it.

There is an interesting theoretical argument suggested in [24], which relates pions and scalar di-quarks in the QCD with two colors. Indeed, in this theory di-quarks are not much heavier than mesons, but are degenerate with them, due to the so called Pauli-Gursey symmetry. In particular, the lowest di-quarks should be bound as strongly as the lowest meson, the massless pions. And indeed, the general pattern of symmetry breaking $SU(2N_f) \rightarrow Sp(2N_f)$ and the number of Goldstone modes is

$$N_{goldstones} = 2N_f^2 - N_f - 1.$$

For the most interesting case $N_f = 2$ there are five massless modes: three pions, plus scalar di-quark S and its

anti-particle \bar{S} . So, in this theory the pions and scalar di-quarks are related by symmetry, and should be truly identical. For three colors it is of course not so, but by continuity in the number of colors, one may expect some traces of that to remain valid.

To get quantitative estimates, we proceed as follows. On the one hand, we evaluate from the ILM the di-quark two-point function,

$$\Pi_{dq}(l) = \langle 0 | J_{sc}^a(x) J_{a\ sc}^\dagger(0) | 0 \rangle, \quad (22)$$

where $J_{sc}^a(x)$ is the scalar current:

$$J_{sc}^a(x) = \epsilon^{abc} u^b(x) (C \gamma_5) d^c(x), \quad (23)$$

and the di-quark three-point function,

$$\Pi_{dq4}(l, l) = \langle 0 | J_{sc}^a(x/2) J_4^{em}(y) J_{a\ sc}^\dagger(-x/2) | 0 \rangle, \quad (24)$$

and obtain the ratio $\Gamma_{dq}(l) := \Pi_{dq4}(l, l) / \Pi_{dq}(l)$.

On the other hand, we compute the spectral decomposition for the same quantities, as if the di-quark be a physical (scalar) particle. This assumption was discussed in detail in [12], where the mass of the di-quark was also determined from the RILM to be $M_{dq} = 420 \pm 30 \text{ MeV}$. As in the case of the nucleon, the large distance limit of the spectral decomposition of the three-point function requires the knowledge of the form-factor of lowest lying state. Exploiting the similarities between the physical properties of the pion and those of the di-quark in the ILM, we take a mono-pole shape ansatz for its form-factor,

$$F_{dq}(Q^2) = \frac{1}{1 + \frac{Q^2}{\alpha}}. \quad (25)$$

The free parameter α can be determined by comparing the function Γ_{dq} evaluated (at large distances) from ILM and from the spectral decomposition (see fig. 11) we found $\alpha \sim (1700 \text{ MeV})^2$.

Clearly, the agreement of ILM prediction with the pole contribution to the spectral representation (obtained using (25)) is definitely worse for the scalar di-quark than for the pion [16], indicating that the simple mono-pole ansatz (25) does not quite work in the case of the di-quark. Of course this should not surprise: after all, the di-quark is not an asymptotic state and we expect its charge distribution to be somewhat distorted by the presence of the third quark.

⁶To remind the reader about importance of these correlation: in IILM topological charge is screened and topological susceptibility is small, $O(m_q)$, as in the QCD vacuum with light quarks. In RILM it is large, like in gluodynamics (quenched QCD).

⁷Note that this feature is similar to what has been found for the pion form-factor in [16].

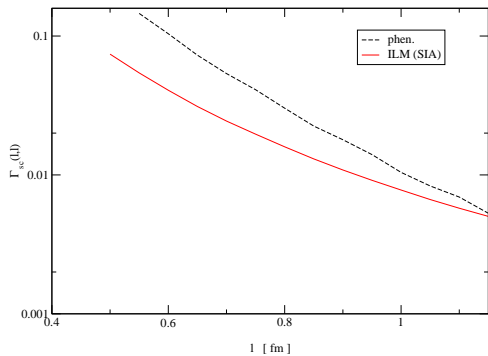


FIG. 11. The ratio $\Gamma_{sc4}(l, l)$ evaluated in the ILM, SIA (solid line) and from the ansatz (25) with $\alpha = 1760 MeV$ (dashed line).

Nevertheless, from this fit we can still obtain a qualitative estimate of its size from the usual relation:

$$\langle r^2 \rangle := 6 \left(\frac{dF_{dq}(q^2)}{dq^2} \right) = \frac{6}{\alpha^2} \simeq 0.3 fm. \quad (26)$$

This value can, for instance, be compared with the phenomenological quark-diquark model [15], where the value $\langle r_{dq}^2 \rangle \simeq (0.45 fm)^2$ was found.

Although both values can only be considered as qualitative estimates, they seem to indicate that the size of the di-quark is of the same order of the typical size of an instanton.

V. CONCLUSIONS AND OUTLOOK

In this paper we have studied the instanton contribution to the proton's electro-magnetic form-factors. We have calculated the ratio $\Gamma_{sc}(l)$ of the proton electro-magnetic three-point function (1) and the two-point function (6) in the RILM, in the IILM and, analytically, in the SIA. It is important to stress that there is no free parameters and therefore the results of fig. 3 represent an absolute prediction for this Green function. Furthermore, the results happen to be independent on the details of the model, and (like it was previously found for the pion form-factor) only the instanton mean radius $\rho \sim 1/600 Mev$ is actually setting the scale of it.

We have compared our theoretical predictions with the phenomenological curve obtained from the nucleon's pole contribution to spectral representation of the correlation functions. In particular, in order to evaluate the proton contribution to the electro-magnetic three-point function we have used several fits of the $G_E \mu / G_M$ data. These fits describe scenarios in which such ratio reaches different asymptotic values, in the kinematical region under current investigation at JLAB. We found that our prediction, is consistent with the deviation from the dipole shape of G_E and is very much in agreement with a scenario in which the $G_E \mu / G_M$ ratio stabilizes somewhere around 0.6, at high Q^2 .

We have also performed a similar analysis to obtain a qualitative estimate of the size of the di-quark part of the nucleon. We found $\langle r^2 \rangle \sim (0.3 fm)^2$, which is consistent with the picture in which quark-zero modes are localized around the closest instanton and in reasonable agreement with the value $\langle r^2 \rangle \sim (0.45 fm)^2$ found in [15].

Our analysis revealed that, although the RILM and the IILM give in general quite different correlators, their prediction for the ratio $\Gamma(l)$ is exactly the same. This implies that at the moment of scattering two out of three quarks interact essentially with one instanton, via its zero mode. This particular configuration is, in a way, at a core of quark-diquark model.

As we found that it is quite possible to perform an analysis of the pion and proton form-factor in the simplest SIA, without needing to model the continuum contribution, one can hope that such analytical results can be Fourier transformed to momentum space and allow for direct comparison with experimental data. We intend to exploit this possibility in our further works.

ACKNOWLEDGMENTS

We would like to thank T.Schäfer for several discussions and numerical help. The work is partly supported by the US DOE grant No. DE-FG02-88ER40388.

**APPENDIX A: DERIVATION OF THE
NUCLEON POLE CONTRIBUTION TO THE
ELECTRO-MAGNETIC THREE-POINT
FUNCTION**

We want to evaluate the proton's pole contribution to the three-point function:

$$\Pi_{sc4}(x, y) = \langle 0 | Tr [\eta_{sc}(x) J_4^{em}(y) \bar{\eta}_{sc}(0) \gamma_4] | 0 \rangle, \quad (\text{A1})$$

where J_4^{em} is the electro-magnetic current:

$$J_4^{em}(y) := \frac{2}{3} \bar{u}(y) \gamma_4 u(y) - \frac{1}{3} \bar{d}(y) \gamma_4 d(y), \quad (\text{A2})$$

and we have chosen $x_4 \geq y_4 \geq 0$.

We begin by inserting two complete sets of states:

$$\begin{aligned} \Pi_{sc4}(x, y) &= \sum_{\Gamma'} \sum_{\Gamma} Tr \left[\langle 0 | \eta_{sc} \left(\frac{x}{2} \right) | \Gamma' \rangle \right. \\ &\quad \left. \langle \Gamma' | J_4(y) | \Gamma \rangle \langle \Gamma | \bar{\eta}_{sc} \left(-\frac{x}{2} \right) | 0 \rangle \gamma_4 \right]. \quad (\text{A3}) \end{aligned}$$

The term of this double sum that depends only on the lowest lying state (nucleon) represents the pole, while the sum of all other terms forms the continuum. We therefore obtain:

$$\begin{aligned} \Pi_{sc4}(x, y) &= \sum_{s, s'} \int \frac{d^3 p'}{2 \omega_{p'} (2\pi)^3} \int \frac{d^3 p}{2 \omega_p (2\pi)^3} \\ &\quad \cdot Tr \left[\langle 0 | \eta_{sc} \left(\frac{x}{2} \right) | p', s'; M_N \rangle \cdot \right. \\ &\quad \cdot \langle p', s'; M_N | J_4(y) | p, s; M_N \rangle \cdot \\ &\quad \left. \cdot \langle p, s; M_N | \bar{\eta}_{sc} \left(-\frac{x}{2} \right) | 0 \rangle \gamma_4 \right] + \dots, \quad (\text{A4}) \end{aligned}$$

where M_N denotes the proton's rest mass and the ellipses denote the continuum contribution. Now, using equation (4) and recalling the definition of Pauli and Dirac form-factors,

$$\begin{aligned} &\langle p', s'; M_N | J_\mu(0) | p, s; M_N \rangle = \\ &= \bar{u}(p', s') [\gamma_\mu F_1(Q^2) + \frac{i M_N}{2} \sigma_{\mu\nu} q^\nu F_2(Q^2)] u(p, s), \quad (\text{A5}) \end{aligned}$$

we get:

$$\begin{aligned} \Pi_{sc,4}(x, y) &= \int \frac{d^3 p'}{2 \omega_{p'} (2\pi)^3} \int \frac{d^3 p}{2 \omega_p (2\pi)^3} \Lambda_{sc}^2 \cdot \\ &\quad exp \left[-i \frac{x}{2} (p + p') - i y (p - p') \right] Tr \left[(\not{p}' + M_N) \cdot \right. \\ &\quad \left. \left(\gamma_4 F_1(Q^2) + \frac{i M_N}{2} \sigma_{4\nu} q^\nu F_2(Q^2) \right) (\not{p} + M_N) \gamma_4 \right] + \dots \quad (\text{A6}) \end{aligned}$$

Now we can re-write the form-factors in terms of their Fourier transform,

$$F_1(Q^2) = \int \frac{d^4 z}{(2\pi)^4} e^{i q \cdot z} F_1(z) \quad (\text{A7})$$

$$F_2(Q^2) = \int \frac{d^4 z}{(2\pi)^4} e^{i q \cdot z} F_2(z), \quad (\text{A8})$$

and introduce the expression for the nucleon propagator in coordinate space ($x'_0 \geq x_0$):

$$S_{M_N}(x', x) = \int \frac{d^3 p}{(2\pi)^3 2 \omega_p} e^{-i p \cdot (x' - x)} (\not{p} + M_N), \quad (\text{A9})$$

obtaining:

$$\begin{aligned} \Pi_{sc4}(x, y) &= \Lambda_{sc}^2 \int d^4 z Tr \left[S_{M_N} \left(\frac{x}{2}, y + z \right) \cdot \right. \\ &\quad \left. \left[\gamma_4 F_1(z) + \frac{i \sigma_{4\nu}}{2 M_N} F_2^\nu(z) \right] S_{M_N} \left(y + z, -\frac{x}{2} \right) \gamma_4 \right] + \dots \quad (\text{A10}) \end{aligned}$$

where:

$$F_2^\nu(z) := i \partial^\nu F_2(z). \quad (\text{A11})$$

One can check that the analytic continuation of (A10) to Euclidean space⁸ is real.

-
- [1] Jefferson Laboratory Hall A Collaboration, Phys. Rev. Lett., **84** (2000) 1398.
 - [2] V.A. Matveev, R.M. Muradian and A.N. Tavkhelidze, Rev. Nuovo Cim. Lett. **7** (1973) 719.
 - [3] F.M. Dittes, A.V. Radyushkin, Phys. Lett. **B134** (1984), 359.
 - [4] G.Sterman, P. Stoler, Ann. Rev. Nucl. Part. Sci., **43** 143.
 - [5] M.A. Shifman, A.I. Vainshtein, A.I. Zakharov, Nucl. Phys., **B163** (1980) 46.
 - [6] B. L. Ioffe and A.V. Smilga, Phys. Lett. **B114** (1982) 353; Nucl. Phys. **216** (1983) 373.
 - [7] Y.Chung, H.G. Dosch, M.Kremer and D.Shall, Phys. Lett., **B102** (1981) 175. Y.Chung, H.G. Dosch, M.Kremer and D.Shall, Nucl. Phys., **B197** (1982) 55.
 - [8] V. A. Nesterenko and A. V. Radyushkin, Phys. Lett. **B115**, (1982) 410; JETP Lett. **39**, (1984) 707.
 - [9] T.Schaefer and E.V.Shuryak, Rev. Mod. Phys., **70** (1998) 323.
 - [10] T. Schafer and E. V. Shuryak, Phys. Rev. Lett. **86**, 3973 (2001) [hep-ph/0010116].
 - [11] E.V. Shuryak and J.J.M. Verbaarschot, Nucl. Phys., **B140** (1993) 37.
 - [12] T. Schaefer, E.V. Shuryak and J.J.M. Verbaarschot, Nucl. Phys., **B412** 143 (1994).
 - [13] T. Schaefer and E.V. Shuryak, Phys. Rev., **D54** 1099 (1996).

⁸ In our Euclidean formulation, $x \cdot y = \sum_{\mu=1}^4 x_\mu y_\mu$, $\{\gamma_\mu, \gamma_\nu\} = 2 \delta_{\mu\nu}$, $\gamma_\nu^\dagger = \gamma_\nu$ and $\sigma_{\mu\nu} = \frac{i}{2} [\gamma_\mu, \gamma_\nu]$.

- [14] G. Hellenstern, R. Alkofer, M. Oettel, H. Reinhardt, Nucl. Phys., **A627** (1997) 679.
M. Oettel, R. Alkofer and L. von Smekal, Eur. Phys. J., **A8** (2000), 553.
V. Keiner, Z. Phys., **A359** (1997) 91.
- [15] J.C.R. Bloch, C.D Roberts, S.M. Schmidt, A. Bender, M.R. Frank, Phys. Rev., **C60** (1999) 62.
J.C.R. Bloch, C.D Roberts, S.M. Schmidt, Phys. Rev., **C61** (2000) 065207.
- [16] A. Blotz and E.V. Shuryak, Phys. Rev., **D55** (1997) 4055.
- [17] H. Forkel and M. Nielsen, Phys. Lett., **B345** (1997) 55.
- [18] E.V. Shuryak, Rev. Mod. Phys., **65** (1993) 1.
- [19] A. F. Sill *et al*, Phys. Rev., **D48** (1993) 29.
- [20] E.V. Shuryak, Nucl. Phys., **B214** (1982), 237.
- [21] M.C. Chu, J.M. Grandy, S. Huang and J.W. Negele, Phys. Rev., **D49** (1994) 6039.
- [22] E.V. Shuryak, Nucl. Phys., **B302** (1986) 599.
- [23] P. Faccioli and E. V. Shuryak, hep-ph/0106019
- [24] R. Rapp, T. Schafer, E. V. Shuryak and M. Velkovsky, Phys. Rev. Lett. **81**, 53 (1998) [hep-ph/9711396].